Bioresource Technology 247 (2018) 537–544

Contents lists available at ScienceDirect

Bioresource Technology

journal homepage: www.elsevier.com/locate/biortech

# Effectiveness and mechanisms of phosphate adsorption on iron-modified biochars derived from waste activated sludge

Qi Yang[a,b,*], Xiaolin Wang[a,b], Wei Luo[c], Jian Sun[a,b], Qiuxiang Xu[a,b], Fei Chen[a,b], Jianwei Zhao[a,b], Shana Wang[a,b], Fubing Yao[a,b], Dongbo Wang[a,b], Xiaoming Li[a,b], Guangming Zeng[a,b]

[a] College of Environmental Science and Engineering, Hunan University, Changsha 410082, China
[b] Key Laboratory of Environmental Biology and Pollution Control, Hunan University, Ministry of Education, Changsha 410082, China
[c] Modern Engineering Training Center, Hunan University, Changsha 410082, China

## GRAPHICAL ABSTRACT

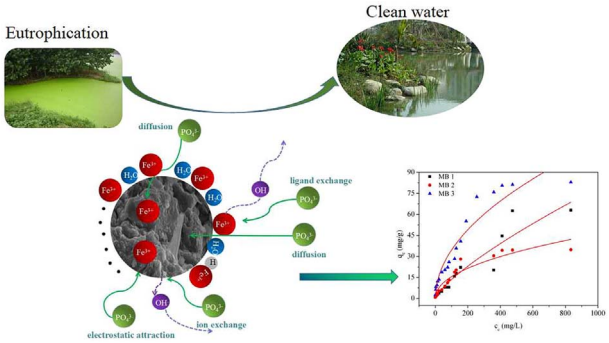


## ARTICLE INFO

*Keywords:*
Adsorption
Biochar
$FeCl_3$-impregnation
Phosphate
Waste activated sludge

## ABSTRACT

Excessive discharge of phosphate (P) into the surface water is the key factor to cause the eutrophication, so its removal has aroused much attention in recent years. In this study, different iron modification (chemical co-precipitation of $Fe^{3+}/Fe^{2+}$ or $FeCl_3$ impregnation) was used to improve the phosphate adsorption capacity of waste activated sludge (WAS)-based biochar. Comparative tests demonstrated that the $FeCl_3$-impregnated WAS-based biochar exhibited much superior phosphate adsorption capacity (111.0 mg/g) in all as-prepared samples and performed well even under the interferences with pH and coexisting ions. X-ray diffraction (XRD) analyzes indicated that the iron in $FeCl_3$-impregnated WAS-based biochar existed mainly in amorphous phase, as hematite and amorphous hydroxides forms, which was of great benefit to the phosphate adsorption. Besides, ligand exchange plays important role in the adsorption of phosphate. The WAS-based biochar kept over 60% phosphate removal efficiency after five recycles.

## 1. Introduction

Eutrophication, caused by the excessive emission of nutrient particularly phosphorous (P), has become a tough environmental problem around the world (Zhao et al., 2015). High level phosphate can stimulate the growth of organisms, especially algae, in water bodies and thus deteriorate the quality of the aquatic ecosystems (Karaca et al., 2004). The natural recovery of phosphate is inefficient because

* Corresponding author at: College of Environmental Science and Engineering, Hunan University, Changsha 410082, China.
*E-mail address:* yangqi@hnu.edu.cn (Q. Yang).

http://dx.doi.org/10.1016/j.biortech.2017.09.136
Received 8 August 2017; Received in revised form 17 September 2017; Accepted 19 September 2017
Available online 22 September 2017
0960-8524/ 

phosphate are temporally converted into sedimentation and then released into waters again (Loganathan et al., 2014). Therefore, it is imperative to explore an efficient technology to remove phosphate from water.

To date, numerous technologies have been investigated to remove phosphorus from wastewaters, which are mainly divided into three categories: chemical, biological and physical methods (Karaca et al., 2004; Wang et al., 2012). Chemical phosphorus removal will generate plenty of sludge due to the precipitation of phosphorus and might potentially result in new pollution (Yao et al., 2011; Yeoman et al., 1988). Biological phosphorus removal is sensitive to the operation parameters, so its efficiency is unstable (Sun et al., 2017; Xie et al., 2017). Moreover, biological treatment involves the waste activated sludge disposal or other pretreatment, which would increase the cost of wastewater treatment (Neufeld and Thodos, 1969). Contrary to other expensive physical methods such as electrodialysis and reverse osmosis (Loganathan et al., 2014), adsorption is low cost and high efficiency. So it has been widely applied in phosphate removal from water (Bhatnagar and Sillanpää, 2011).

Various adsorbents have been used in phosphate removal, such as activated carbon (Loganathan et al., 2014), metal hydroxide (Chitrakar et al., 2005), blast furnace slag (Kumar et al., 2010) and so on. Recently, biochars have been concerned for their broad source, especially that they can be prepared from abundant waste cellulosic materials (Zhong et al., 2012; Zhao et al., 2016). However, the phosphate adsorption capacity of virgin biochar is unfavorable. Michalekova-Richveisova et al. (2017) demonstrated that the maximum phosphate adsorption capacity of three non-modified biochars were very low, which were 0.036 mg/g for corn cobs biochar, 0.132 mg/g for garden wood waste biochar and 0.296 mg/g for wood chips biochar, respectively. In order to improve the phosphate adsorption performance of biochar, iron modification is often employed. Compared with other modified methods, for instance the activation by sulfuric acid (Kumar et al., 2010) and lanthanum (Chouyyok et al., 2010), iron modification had simple and efficient features. It is well known that different iron modification may cause different valence states of iron in biochar. However, the relationship between the phosphate adsorption efficiency and valence states of iron existed in the biochar is vague.

In this study, the influence of inert atmosphere on the valence states of iron existed in biochars will be explored. Firstly, biochar derived from waste activated sludge (WAS) was modified by three different methods: co-precipitation of $Fe^{2+}/Fe^{3+}$ under nitrogen atmosphere, co-precipitation of $Fe^{2+}/Fe^{3+}$ under air and impregnation with ferric chloride. Then the properties of three iron-modified biochars were characterized and their phosphate removal efficiency was compared. Lastly, the underlying mechanism was discussed.

## 2. Materials and methods

### 2.1. Materials

The WAS taken from a secondary sedimentation tank of a municipal wastewater treatment plant in Changsha, China was concentrated by settling at 4 °C for several days. After pouring the liquid supernatant, the concentrated sludge was dried in oven at 105 °C and sieved into fine powders for further use.

The phosphate stock solution (1000 mg/L) was prepared by dissolving potassium dihydrogen orthophosphate ($KH_2PO_4$) powders in deionized water and desired solutions were prepared by diluting the phosphate stock solution. All the chemical reagents used in the study are of analytical grade.

### 2.2. Biochar preparation and modification

The virgin biochar, produced by pyrolyzing dewatered sludge at 550 °C without any modification, did not achieve obvious phosphate removal but release 15.88 mg/g phosphate. When immersed by 0.7 M $ZnCl_2$ solution, the phosphate removal rate of biochar raised to 28.5% for 20 mg/L phosphate solution (data not shown). Thus further modification of biochar is necessary.

The WAS-based biochar was generated through an impregnation and pyrolysis process. Briefly, the dewatered sludge powders was soaked with 0.7 M $ZnCl_2$ solution with magnetic stirring for 24 h. The impregnated samples were pyrolyzed in 550 °C and retained for 2 h under nitrogen flow to prepare the biochar. Lastly, the biochar was crushed and sieved to 0.5–1 mm size fraction, washed with deionized water to remove impurities, oven dried at 65 °C and sealed in glass container.

As-prepared biochars were modified by three different iron modification as follows:

(1) Biochar decorated by co-precipitation of $Fe^{2+}/Fe^{3+}$ under nitrogen atmosphere (labeled MB1): Under room temperature and nitrogen atmosphere, 1 g biochar was added into a 30 mL solution, which contained 1.17 g $FeSO_4{\cdot}7H_2O$ and 1.09 g $FeCl_3{\cdot}6H_2O$, stirred vigorously at 150 rpm for several minutes followed by the dropwise adding of NaOH to adjust pH to 11. Aqueous suspension kept stirring for 45 min and aged overnight without stirring. The separated solid was washed several times with deionized water and dried in vacuum drying chamber.
(2) Biochar decorated by co-precipitation of $Fe^{2+}/Fe^{3+}$ under air atmosphere (labeled MB2): The process was same with (1) except that there was no nitrogen protection and the solid was dried in oven.
(3) Biochar decorated by impregnation with ferric chloride under air atmosphere (labeled MB3): The process was same with (2) except that the solution only contained 2.18 g $FeCl_3{\cdot}6H_2O$.

### 2.3. Batch adsorption experiment

The batch adsorption experiments were conducted to determine the phosphate adsorption capacity of three novel biochars. 0.1 g biochars were loaded into a 250 mL Erlenmeyer flask, containing 50 mL of phosphate solutions with the concentration of 20 mg/L. The initial pH was adjusted to 7.0 ± 0.2 by adding 2 M HCl or NaOH. Then Erlenmeyer flasks were shaked at 120 rpm and 22 ± 0.5 °C in a temperature controlled water bath shaker until the adsorption equilibrium. The phosphate adsorption performance was compared by the decrease of the phosphate amount in the solution.

### 2.4. Adsorption isotherm

To examine the adsorption isotherm of the biochar, 0.1 g adsorbent was added into 50 mL phosphate solutions with different initial concentration (5–1000 mg/L). The adsorption capacity at equilibrium was calculated according to Eq. (1):

$$q_e = V \times \frac{(c_e - c_0)}{m} \quad (1)$$

where $q_e$ is the equilibrium adsorption capacity (mg/g), $V$ is the volume of solution (mL), $c_e$ and $c_0$ represent the concentrations at the equilibrium and initial time (mg/L), respectively, and $m$ is the weight of adsorbent (g).

### 2.5. Adsorption kinetics

In this experiment, 0.2 g biochar was loaded into 100 mL phosphate solutions with the concentration of 20 mg/L at room temperatures. The residual phosphate content at different time intervals (0, 5, 10, 20, 40, 60, 90, 120, 240, 720 and 1440 min) was analyzed to determine the adsorption kinetics.

### 2.6. Effect of pH and coexisting anions

The effect of initial pH on adsorption capacity of biochars was investigated at desirable values pH (2.0, 5.0, 7.0, and 9.0) in 20 mg/L phosphate solutions. In order to explore the influence of coexisting anion, 0.01 M of $Na_2SO_4$, $NaNO_3$ or $Na_2CO_3$ was added to 20 mg/L phosphate solutions to measure the phosphate adsorption performance of biochar.

### 2.7. Analytical methods

The phosphate concentrations in the solution were examined by the ascorbic acid method (ESS Method 310.1) (USEPA, 1992). Fourier transform infrared spectrometer (FTIR) spectra were recorded by an IR Prestige-21 spectrometer (Shimadzu, Japan). The porosity and surface characteristics of biochar were measured by $N_2$ adsorption at 77 K on a TRISTAR-3000 surface area analyzer. Power X-ray diffraction (XRD) was measured on a Rigaka D/max 2500 v/pc. Zeta potential of biochars was determined by a zeta potential analyzer.

Experimental results were indicated as mean ± standard deviation. The average was calculated from three replicates of each experimental treatment. The analysis of variance of data was used and it was acceptable when p was less than 0.05.

## 3. Results and discussion

### 3.1. Characterization of modified biochars

#### 3.1.1. Surface and porous characteristic

Table 1 lists the surface and porous characteristics of as-prepared samples. As shown in Table 1, the surface area of virgin biochar without any modification was very low (1.533 $m^2/g$), which can be remarkably improved after immersed with $ZnCl_2$ solution (184.409 $m^2/g$). The biochars treated by $ZnCl_2$ presented smaller pore diameter (< 1 nm) than that of original sample, resulting in satisfactory adsorption ability (Sarkar et al., 2011). That maybe attribute to the strong dehydrator function and porogen potential of $ZnCl_2$ (Kim et al., 2001). After being treated by the iron solution, the surface area of biochars was further improved except MB1, which demonstrated that pyrolysis made the biochar (MB2 and MB3) be washed to a certain extent, increasing the inner space in biochar. Contrarily, inert gas atmosphere well protected the structure of biochar (MB1). Besides, the modified biochar also performed well-developed porous structure. The total pore volume of all modified biochars was larger than that of the virgin, which was in favor of improving the adsorption capacity (Loganathan et al., 2014). The above results suggested that the modified biochars possessed good adsorption capacity due to their superior feature in surface area and porous structure (Zhang et al., 2012).

#### 3.1.2. XRD

XRD analyzes were carried out to study the crystalline structure of modified biochars and the results are shown in Fig. 1A. Apparently, there was a common diffraction peak at 2θ values of 26°, which was indexed as amorphous nature of carbon (Mohan et al., 2011). Although

**Table 1**
Surface and pore structure parameters of samples.

| | Virgin biochar | Immersed with $ZnCl_2$ | MB1 | MB2 | MB3 |
|---|---|---|---|---|---|
| BET surface area ($m^2/g$) | 1.533 | 184.409 | 156.788 | 226.015 | 254.400 |
| Total pore volume ($cm^3/g$) | 0.338 | 0.741 | 1.018 | 1.096 | 0.889 |
| Pore diameter (nm) | 0.983 | 0.889 | 0.888 | 0.889 | 0.887 |

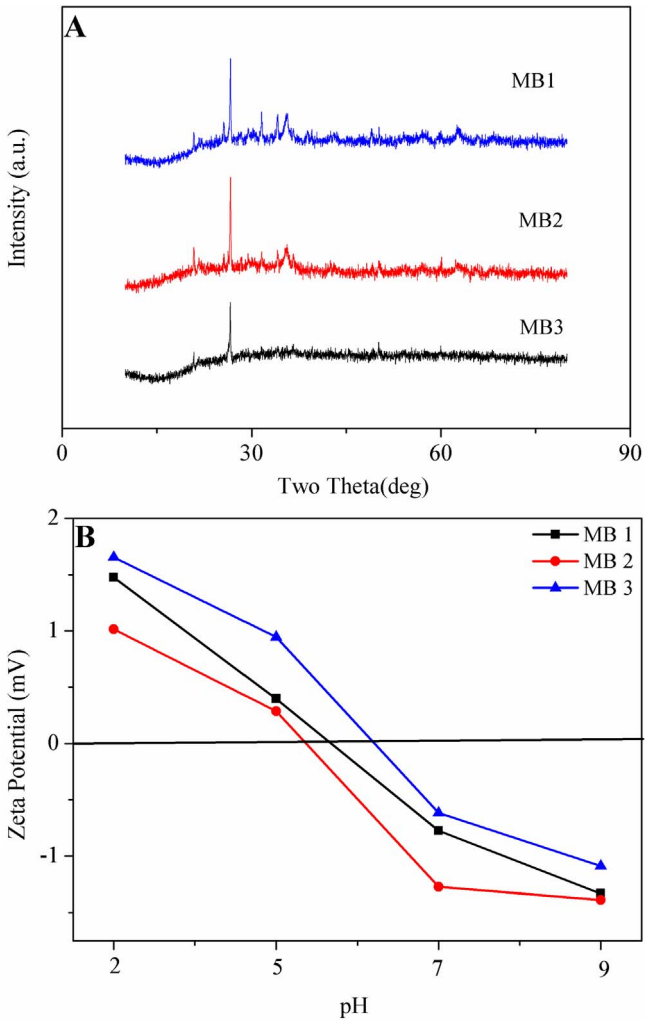


**Fig. 1.** XRD patterns (A) and zeta potential (B) of three novel biochars. MB1: modified by co-precipitation of $Fe^{2+}/Fe^{3+}$ under nitrogen atmosphere. MB2: modified by co-precipitation of $Fe^{2+}/Fe^{3+}$ under air. MB3: modified by $FeCl_3$ impregnation.

the crystalline structure of three modified biochars was not good, MB1 was better among them. There were three obvious peaks at 2θ values of 30.2°, 35.3° and 36.2° in the spectrum of MB1, which were coincident with the phase of γ-$Fe_2O_3$ and the spinel structure of $Fe_3O_4$ phase, respectively (Han et al., 2016; Osouli-Bostanabad et al., 2015). In the spectrum of MB2, the peak at 2θ values of 35.5°,39.09° indicated the presence of γ-$Fe_2O_3$ (Han et al., 2016) and $Fe(OH)_2$ (Mohan et al., 2011). There was an inconspicuous peak at 60.7° for MB2 and MB3, suggesting the existence of $Fe(OH)_3$ (Mohan et al., 2011) in two modified biochars. There was no obvious peak at 2θ values of 30°–70° in the spectrum of MB3, suggesting the iron took the form of amorphous phase in MB3, which was more beneficial than crystalline iron oxides in adsorption of phosphate (Zeng et al., 2004). Above characterization results confirmed that impregnation process may influence the crystallinity of materials (Krishnan and Haridas, 2008).

#### 3.1.3. FTIR

The surface functional groups on the modified biochars were determined by FTIR analysis. Corresponding spectra of biochars are summarized in Supplementary data. All biochars showed some bands at around 3448 $cm^{-1}$ and 1630 $cm^{-1}$, which attributed to the–OH stretching vibrations or the sorbed water molecules and water deformation (Yan et al., 2015), respectively. Besides, there was a common peak at 2325 $cm^{-1}$, representing the goethite ($Fe_2O_3{\cdot}H_2O$) (Cambier, 1986). The band around 454 $cm^{-1}$ and 1067 $cm^{-1}$, representing

hematite and Fe-OH, were also found in three biochars, indicating that the iron was immobilized on the biochars (Krishnan and Haridas, 2008; Ruan et al., 2002). The peak of Fe-O (580–620 $cm^{-1}$) was found in MB1 and MB2 (Lim et al., 2009). These iron oxides and metal hydroxyl groups may play an important role in attraction of phosphate as the active adsorption sites (Ren et al., 2015; Zhang et al., 2009).

#### 3.1.4. Zeta potential

Zeta potential of three modified biochars is illustrated in Fig. 1B. Apparently, the tendency of three biochars was similar: the zeta potential all decreased as pH increased. When pH was lower than 6, zeta potential was positive, which was desirable to the adsorption of anion by electrostatic attraction. With pH increasing, the zeta potential became negative and it is adverse to the anion adsorption. Noticeably, MB3 exhibited the highest zeta potential among three biochars, which maybe one of the useful reason to explain its excellent adsorption ability.

### 3.2. Adsorption isotherms

In this study, Freundlich (Eq. (2)) and Langmuir (Eq. (3)) adsorption isotherms were used to investigate the adsorption performance of phosphate on three novel biochars and the results were illustrated in Table 2.

$$q_e = K_F \times C_e^{1/n} \tag{2}$$

$$\frac{c_e}{q_e} = \frac{c_e}{q_{max}} + \frac{1}{K_L \times q_{max}} \tag{3}$$

where $q_e$ is the adsorption capacity at equilibrium (mg/g), $c_e$ is the phosphate concentration at equilibrium (mg/L). $K_F$ ($\mu g \cdot g^{-1}$) and $n$ are Freundlich constants. $q_max$ represents the maximum adsorption capacity (mg/g) of adsorbents.$K_L$ is the Langmuir constant.

As can be seen from Table 2 and Fig. 2, the experimental data of three biochars was fitted well to Freundlich isotherms ($R^2 > 0.9$), indicating the surface of adsorbent was heterogeneous (Cui et al., 2016). Besides, the value of $1/n$ was greater than 1, suggesting the cooperative adsorption in the present study (Krishna Veni et al., 2017). Compared with the isotherm parameters, MB3 performed excellent adsorption ability in all investigated phosphate concentration range, correspondingly, MB1 only displayed better adsorption performance in high P-containing solution. The maximum phosphate adsorption capacity of MB3 calculated by Langmuir model was 111.0 mg/g, which is obviously greater than that of the adsorbent reported in previous researches (Table 3). Thus, MB3 was selected for the further experiments. Besides, it is noticed that when MB3 was applied into low concentration phosphate, even lower than 5 mg/L, the phosphate removal rate could reach to 98%, suggesting its feasibility to the removal of low concentration phosphate from surface water.

### 3.3. Adsorption kinetics

Adsorption kinetics is usually used to estimate the rate of adsorption, which is an important characteristic to identify the adsorption performance of adsorbent. As shown in Fig. 3A, when the initial phosphate concentration was 20 mg/L, rapid adsorption was observed in the first 60 min, which suggested that P in solution was impelled to adhere on the surface of biochar by the electrostatic attraction. Then, the adsorption rate slowed since that ion exchange and ligand exchange controlled the following adsorption process.

In this study, the experimental data were simulated by pseudo-first-order and pseudo-second- order kinetic models, respectively. The kinetic models can be expressed as:

$$lg(q_e - q_t) = lg\, q_e - K_1 \times \frac{t}{2.303} \tag{4}$$

$$\frac{t}{q_t} = \frac{1}{K_2 \times q_e^2} + \frac{t}{q_e} \tag{5}$$

where $q_e$ and $q_t$ denote the adsorbed amount of phosphate (mg/g) at equilibrium and at time t, respectively. $K$ is the kinetic constant.

The kinetic parameters listed in Table 4 showed that the fitting of pseudo-second-order model was more satisfactory, which indicated that the phosphate adsorption on biochars was conducted through the inner sphere complex (Wang et al., 2011). Some studies have reported that intraparticle surface diffusion may play an important role in the transportation of adsorbate in adsorbent, and Weber-Morris modle was generally used to verify this process (Yao et al., 2011). According to the relationship between the adsorbed P ($q_t$) and the square root of time

**Table 2**
Langmuir and Freundlich parameters for phosphate adsorption on different biochars.

| Modle | Parameter 1 | Parameter 2 | $R^2$ |
|---|---|---|---|
| *Langmuir* | | | |
| MB1 | $K_L$ = 9.91 L/mg | $q_{max}$ = 61.2 mg/g | 0.9087 |
| MB2 | $K_L$ = 8.15 L/mg | $q_{max}$ = 34.2 mg/g | 0.9188 |
| MB3 | $K_L$ = 3.02 L/mg | $q_{max}$ = 111.0 mg/g | 0.9395 |
| *Freundlich* | | | |
| MB1 | $K_F$ = 2.98 $mg^{(1-1/n)}$ $L^{1/n}$/g | 1/n = 1.35 | 0.9289 |
| MB2 | $K_F$ = 2.80 $mg^{(1-1/n)}$ $L^{1/n}$/g | 1/n = 1.33 | 0.9656 |
| MB3 | $K_F$ = 0.02 $mg^{(1-1/n)}$ $L^{1/n}$/g | 1/n = 2.38 | 0.9472 |

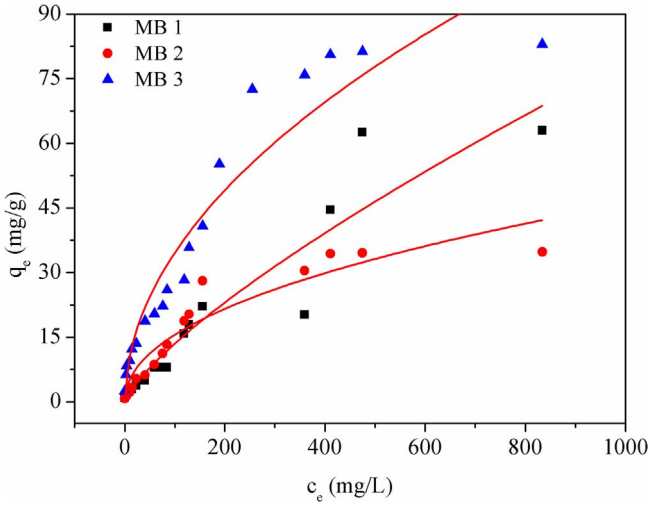


**Fig. 2.** Freundlich plot for phosphate adsorption on biochars. MB1: modified by co-precipitation of $Fe^{2+}/Fe^{3+}$ under nitrogen atmosphere. MB2: modified by co-precipitation of $Fe^{2+}/Fe^{3+}$ under air. MB3: modified by $FeCl_3$ impregnation.

**Table 3**
P adsorption capacity of different adsorbents.

| Adsorbent | Q (mg/g) | Reference |
|---|---|---|
| Dewatered alum sludge | 3.50 | Zeng et al. (2004) |
| $ZnCl_2$-activated coir-pith carbon | 5.10 | Yeoman et al. (1988) |
| Magnetic orange peel | 1.24 | Kumar et al. (2010) |
| Magnetic water hyacinth biochar | 5.07 | Yan et al. (2015) |
| Fe-impregnated wood chip biochar | 3.20 | Han et al. (2016) |
| Magnetite Nanoparticles | 5.30 | Zhang et al. (2009) |
| Fe (II)-doped activated carbon | 14.12 | Yao et al. (2011) |
| Fe (III)-doped activated carbon | 8.13 | Yao et al. (2011) |
| $Fe^{3+}/Fe^{2+}$ modified WAS biochar under $N_2$ atmosphere | 61.20 | This study |
| $Fe^{3+}/Fe^{2+}$ modified WAS biochar without $N_2$ atmosphere | 34.20 | This study |
| Iron-impregnated WAS biochar | 111.00 | This study |

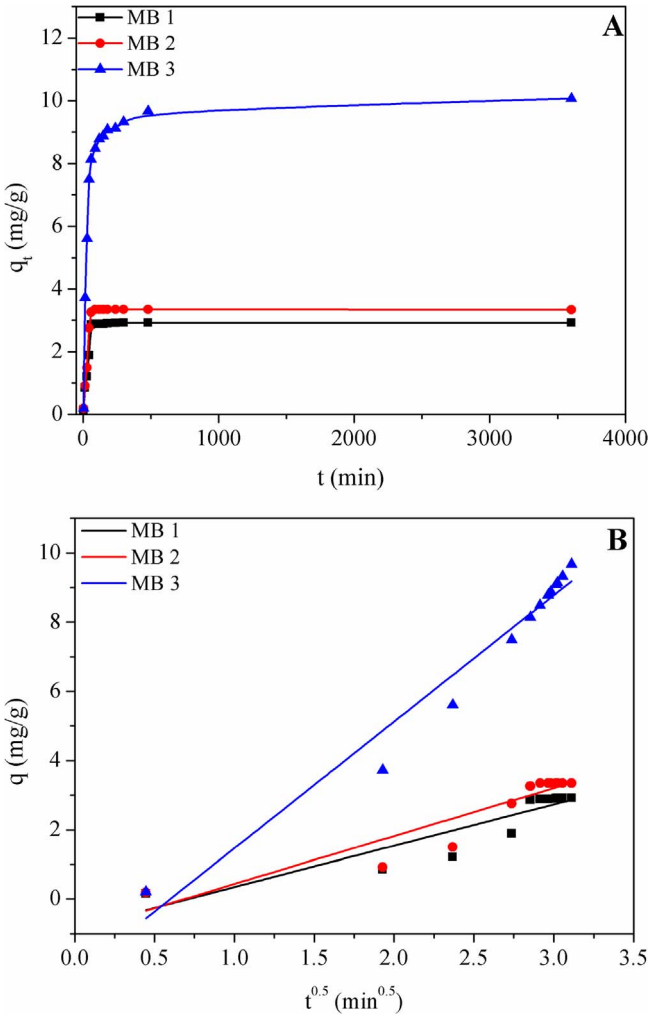


**Fig. 3.** Time courses of phosphate adsorption on different biochars (A) and linear fitting curves of the Weber-Morrismodle (B). MB 1: modified by co-precipitation of $Fe^{2+}/Fe^{3+}$ under nitrogen atmosphere. MB 2: modified by co-precipitation of $Fe^{2+}/Fe^{3+}$ under air. MB 3: modified by $FeCl_3$ impregnation.

**Table 4**
Kinetic parameters for phosphate adsorption on different biochars.

| Modle | Parameter 1 | Parameter 2 | $R^2$ |
|---|---|---|---|
| *First-order* | | | |
| MB1 | $K_1$ = 0.025/h | $q_e$ = 2.92 mg/g | 0.8622 |
| MB2 | $K_1$ = 0.078/h | $q_e$ = 3.34 mg/g | 0.8973 |
| MB3 | $K_1$ = 0.012/h | $q_e$ = 10.07 mg/g | 0.8365 |
| *Second-order* | | | |
| MB1 | $K_2$ = 0.018 g/(mg·min) | $q_e$ = 2.94 mg/g | 0.9992 |
| MB2 | $K_2$ = 0.019 g/(mg·min) | $q_e$ = 3.36 mg/g | 0.9993 |
| MB3 | $K_2$ = 0.005 g/(mg·min) | $q_e$ = 10.13 mg/g | 0.9992 |

($t^{0.5}$), it was explored whether intraparticle surface diffusion was the predominate factor in adsorption. In this work, experimental data fitted well ($R^2 > 0.9$) to Weber-Morris modle, suggesting the importance of intraparticle diffusion in phosphate adsorption on the modified biochars (Fig. 3B).

### 3.4. Effects of pH on P removal

Fig. 4 represents the effect of pH on the phosphate removal efficiency by three biochars. It can be seen that the phosphate removal efficiency (adsorption capacity) of MB1, MB2 and MB3 was 58.9%

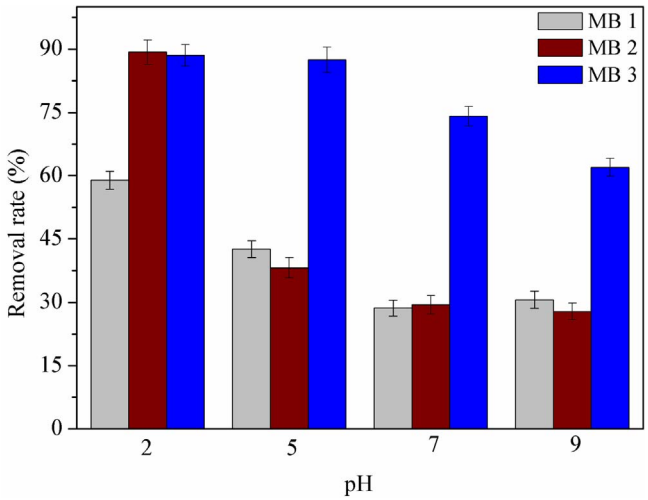


**Fig. 4.** The removal rate of phosphate by three biochars at different pH (initial P concentration: 20 mg/L). MB 1: modified by co-precipitation of $Fe^{2+}/Fe^{3+}$ under nitrogen atmosphere. MB 2: modified by co-precipitation of $Fe^{2+}/Fe^{3+}$ under air. MB 3: modified by $FeCl_3$ impregnation.

(5.7 mg/g), 89.3% (8.6 mg/g) and 88.5% (8.5 mg/g), respectively, at initial pH 2.0 and phosphate concentration 20 mg/L. When the initial pH increased to 7, the corresponding values declined to 28.7% (2.6 mg/g), 29.4% (2.6 mg/g) and 74.1% (8.3 mg/g) respectively. The performance of MB3 was affected very little by initial pH. However, the phosphate adsorption on MB1 and MB2 was highly pH dependent. They all showed excellent phosphate adsorption ability at pH 2. With pH further increasing, their removal efficiency decreased sharply. Above observation suggested that MB 3 was more appropriate to remove phosphate in wide pH range.

Theoretically, when pH is under 2.15, the dominant form of P in solution is $H_3PO_4$. The form of P presents as $H_2PO_4^-$ at pH 2.15–7.20, and the main form changes to $HPO_4^{2-}$ when pH is between 7.2 and 12.33. So $H_3PO_4$ and $H_2PO_4^-$ are the main species of phosphate at low pH, and $H_2PO_4^-$ is the main ion to attract the adsorption site on biochar. Besides, ligand exchange between the unprotonated $H_2PO_4^-$ and the $OH^-$ existed on the surface of biochars is recognized as a promising mechanism for phosphate adsorption and the process was as follows:

$$MB3\text{–}Fe\text{–}OH + H_2PO_4^- + H^+ \rightarrow MB3\text{–}Fe(H_2PO_4) + H_2O \quad (6)$$

When pH is lower than 6, zeta potential of modified biochars are positive (Fig. 1B), which is help to adsorb $H_2PO_4^-$ due to the electrostatic attraction. In alkaline condition, the high concentration of $OH^-$ competes with phosphate for the adsorption site. Moreover, the surface of biochar was negatively charged with pH increasing, which intensified the electrostatic repulsion between phosphate and the biochar, consequently resulting in poor phosphate adsorption.

### 3.5. Effects of coexisting anions on P removal

There often exist simultaneously some ions such as sulfate ($SO_4^{2-}$), nitrate ($NO_3^-$), and carbonate ($CO_3^{2-}$) in actual wastewater, which may potentially interfere to the adsorption of phosphate. Thus, the competitive adsorption experiment was conducted and the results are illustrated in Fig. 5. Although the coexisting ion concentration (0.01 M) was higher than that of phosphate, $SO_4^{2-}$ and $NO_3^-$ had no remarkable effect on the adsorption of phosphate, indicating that there were low competitions between these two ions and phosphate for the active site on MB3. The underlying mechanism of phosphate adsorption occurred in oxides and hydroxides are ligand exchange, which formed the innersphere complexes (Loganathan et al., 2014). According to the experiment result, it could be speculated that the adsorption of $SO_4^{2-}$ and $NO_3^-$ belonged to nonspecifical adsorption and generated the

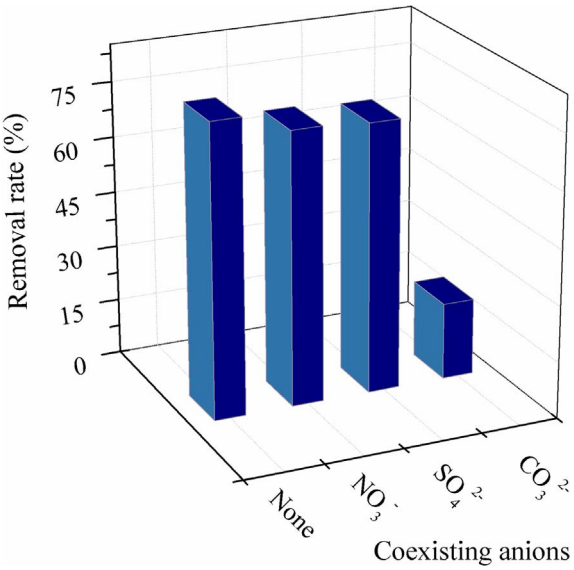


**Fig. 5.** Effect of coexisting anions on phosphate adsorption on MB3.

outersphere complexes, which could not interfere the adsorption of phosphate (Loganathan et al., 2014). However, in the presence of $CO_3^{2-}$, the removal efficiency of phosphate decreased to about 20.61%. The phenomenon illustrated that $CO_3^{2-}$ could compete strongly with phosphate for the adsorption sites on biochar.

### 3.6. Evaluation of phosphate desorption and reuse of adsorbent

An ideal adsorbent is not only high-effective and cost-efficient but also can easily desorb and maintain high adsorption efficiency after recycling. In this study, desorption was carried out by shaking the spent biochar in 100 mL of 0.01 M KCl or 0.25 M NaOH solution. The phosphate desorption capacity was poor in KCl solution (3.2%) but was excellent in NaOH solution (96.7%). Neutral salts such as KCl and NaCl can desorb phosphate from some adsorbents when the bonding between adsorbent and P was weak, which could illustrate that the adsorption mechanism is nonspecific (Xu et al., 2011). In NaOH solution, better phosphate desorption efficiency was achieved because $OH^-$ radicals with strong affinity ability to occupy the limited active sites of biochar. However, a part of phosphate bonded strongly and went to deep inside of the adsorbents, thus the desorption efficiency could not reach to 100% (Genz et al., 2004).

The biochar desorbed by NaOH was separated from the solution and washed with ultrapure water until neutral for recycling. The phosphate adsorption capacity of biochar decreased from 74.09% to 60.03% after 5 successive recycles. Corresponding results are summarized in supplementary materials. It demonstrated that there were some attractive sites that could not be completely reversed during desorption process. Genz et al. (2004) reported that after a long-term adsorption, phosphate may locate in deep inside and attached strongly with adsorbents, resulting in the decrease of available active adsorption site. Although the adsorption capacity of biochar declined with recycling time, the phosphate removal efficiency was higher than 60% after 5 successive recycles, suggesting that WAS-based biochar modified by iron had high reusability and was a promising adsorbent for the phosphate removal.

### 3.7. Adsorption mechanism

#### 3.7.1. Previous study

The iron modified method is an economical and efficient way to improve the phosphate adsorption on biochar. Ren et al. (2015) explored the phosphate adsorption capacity of cotton stalk biochar modified by granulation and chemical precipitation of ferric oxides. They found that the function of iron modification mainly was to change the surface and porous structure of biochar and provide more attractive sites, which improved the phosphate adsorption capacity of biochar. The reaction principle for the chemical co-precipitation of $Fe^{3+}/Fe^{2+}$ to decorate the biochars is expressed as following:

$$Fe^{2+} + 2Fe^{3+} + 8OH^- \rightarrow Fe_3O_4 + 4H_2O \quad (7)$$

In this process, the biochar surface was beneficial to nucleate iron oxide precipitation (Hug et al., 2001). Chen et al. (2011) investigated the phosphate adsorption properties of orange peel biochar, which was decorated by co-precipitation of $Fe^{2+}/Fe^{3+}$ at alkaline condition under air and then pyrolyzed at different temperature. The biochar pyrolyzed at higher temperature exhibited better phosphate removal rate, because that the higher pyrolyzed temperature, the less iron oxide left. However, the valence states of iron in biochar were not investigated. Research showed that the atmosphere of $Fe^{2+}/Fe^{3+}$ co-precipitation had significant impact on the valence states of iron in biochar (Hug et al., 2001). $Fe^{2+}$ is unstable and easily oxidized under air, so the inert gases usually were used to protect $Fe^{2+}$ in some experiments. Shang et al. (Shang et al., 2016) modified pyrolyzed *Astragalus membranaceus* herb residue biochar by co-precipitation of $Fe^{2+}/Fe^{3+}$ under alkaline condition with nitrogen atmosphere. They observed that the crystalline of $Fe_3O_4$ and $Fe_2O_3$ was formed well and the improved chromium adsorption capacity should attribute to the oxygen-containing groups existed in the biochar. It was clearly demonstrated that inert atmosphere favored the generation of $Fe_3O_4$, which may play an important role in adsorption.

#### 3.7.2. Mechanism in the present study

To further elucidate the mechanism of phosphate adsorption on iron modified biochars, it is necessary to investigate the valence state of iron existed in the biochars. In this study, during the co-precipitation process, besides $Fe_3O_4$ being formed, $Fe(OH)_3$ and $Fe(OH)_2$ precipitated in order with pH rising. And $Fe(OH)_2$ can be oxidized to $Fe(OH)_3$ and $Fe_2O_3$ in aqueous phase and in oven, respectively:

$$2Fe(OH)_2 + 1/2O_2 + H_2O \rightarrow 2Fe(OH)_3 \quad (8)$$

$$2Fe(OH)_2 + 1/2O_2 \rightarrow Fe_2O_3 + 2H_2O \quad (9)$$

Water molecule in $Fe(OH)_3$ will be lost when they are heated between 40 °C and 170 °C (Geankoplis, 2003). Therefore, there are $Fe(OH)_3$ and $Fe_2O_3$ existed in the MB2 and MB3. Because being produced in inert gas atmosphere, iron in MB1 existed in the form of $Fe_3O_4$, $Fe_2O_3$ and $Fe(OH)_3$. Previous studies have reported that amorphous hydroxides represented excellent adsorption ability due to their high isoelectric point (Pierce and Moore, 1982). The XRD results showed that the iron took the form of amorphous phase in MB3, so it also exhibited best phosphate adsorption capacity in as-prepared biochars.

The amount of iron in the biochar also played an important role in adsorption process. In this study, the amount of iron impregnated is reflected by the iron concentration in the residual supernatant. The concentration of iron in the residual supernatant for MB1 was the highest (3.78 mg/L), which was almost 4 and 8 folds than that of MB2 and MB3. Therefore, MB1 contained the least iron element and the results were accordance with the previous report that the amount of iron impregnated was the lowest when no oxidant was present (Gu et al., 2005). There was more ferric iron existed in MB3, thus it performed better in phosphate removal.

Compared with the FTIR spectroscopy of raw biochars, the remarkably change for the spent biochars was that the peak at 870 $cm^{-1}$ (Fe–OH) was weaker but peak at 1050 $cm^{-1}$(P–O) appeared, indicating that the group of –OH was replaced by P (Zhang et al., 2009). Furthermore, the adsorption intensity of peak at 454 $cm^{-1}$ (hematite) in MB3 was largely weakened after adsorption, which maybe the main reason for phosphate removal.

Based on the above analysis, it could be concluded that although the

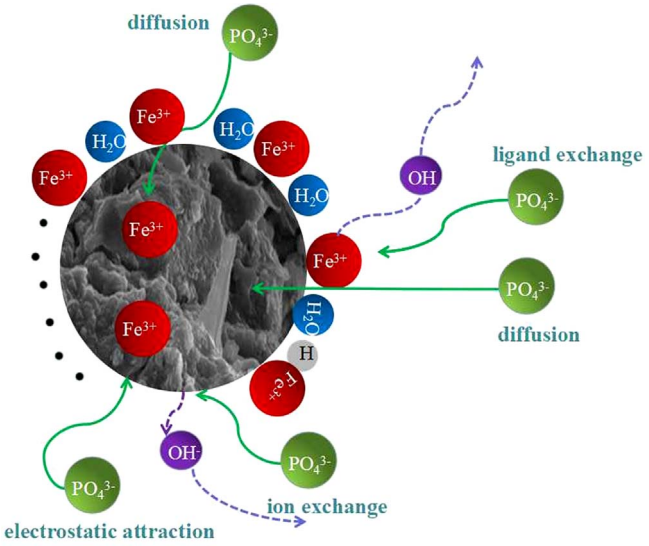


**Fig. 6.** Schematic illustration of the phosphate adsorption on iron-modified biochar.

protection of inert atmosphere was benefit to the generation of $Fe_3O_4$, the attachment of iron to biochar became difficult without the oxidant. Besides, the phosphate removal efficiency of biochar decorated by Fe $(OH)_3$ and $Fe_2O_3$ were better than that by $Fe_3O_4$ and $Fe(OH)_2$. The schematic mechanism dominated the phosphate adsorption on iron modified biochar is illustrated in Fig. 6.

## 4. Conclusion

Iron modified biochar was prepared through the pyrolysis of waste activated sludge and decorated by different modification (chemical co-precipitation of $Fe^{2+}/Fe^{3+}$ or $FeCl_3$ impregnation). The valence state of iron existed in the biochar had significantly different and affected the phosphate removal performance. The maximum phosphate adsorption capacity of biochar decorated by $FeCl_3$ reached to 111.0 mg/g. The phosphate removal efficiency maintained higher than 60% even after 5 successive recycles. Meanwhile, the biochar possessed excellent adsorption ability to low concentration phosphate. High adsorption capacity of $FeCl_3$-modified biochar makes it a promising sorbent for phosphate removal from aqueous solutions.

## Acknowledgements

This research was financially supported by the project of National Natural Science Foundation of China (Nos. 51478170, 51508178, 51779088, 51709104) and Hunan Provincial Natural Science Foundation of China (No. 2017JJ2051)

## Appendix A. Supplementary data

Supplementary data associated with this article can be found, in the online version, at http://dx.doi.org/10.1016/j.biortech.2017.09.136.

## References

Bhatnagar, A., Sillanpää, M., 2011. A review of emerging adsorbents for nitrate removal from water. Chem. Eng. J. 168, 493–504.
Cambier, P., 1986. Infrared study of goethites of Varying crystallinity and particle size: i. interpretation of OH and lattice vibration frequencies. Clay Miner. 21, 191–200.
Chen, B.L., Chen, Z.M., Lv, S.F., 2011. A novel magnetic biochar efficiently sorbs organic pollutants and phosphate. Bioresour. Technol. 102, 716–723.
Chitrakar, R., Tezuka, S., Sonoda, A., Sakane, K., Ooi, K., Hirotsu, T., 2005. Adsorption of phosphate from seawater on calcined MgMn-layered double hydroxides. J. Colloid Interface Sci. 290, 45–51.
Chouyyok, W., Wiacek, R.J., Pattamakomsan, K., Sangvanich, T., Grudzien, R.M., Fryxell, G.E., 2010. Phosphate removal by anion binding on functionalized nanoporous sorbents. Environ. Sci. Technol. 44, 3073–3078.
Cui, X.Q., Dai, X., Khan, K.Y., Li, T.Q., Yang, X.E., He, Z.L., 2016. Removal of phosphate from aqueous solution using magnesium-alginate/chitosan modified biochar microspheres derived from Thalia dealbata. Bioresour. Technol. 218, 1123–1132.
Geankoplis, C.J., 2003. Transport processes and separation. Process Principles, fourth ed. Prentice Hall, NJ.
Genz, A., Kornmuller, A., Jekel, M., 2004. Advanced phosphorus removal from membrane filtrates by adsorption on activated aluminum oxide and granulated ferric hydroxide. Water Res. 38, 3523–3530.
Gu, Z.M., Feng, J., Deng, B.L., 2005. Preparation and evaluation of GAC-based iron-containing adsorbents for arsenic removal. Environ. Sci. Technol. 39, 3833–3843.
Han, Y.T., Cao, X., Ouyang, X., Sohi, S.P., Chen, J.W., 2016. Adsorption kinetics of magnetic biochar derived from peanut hull on removal of Cr (VI) from aqueous solution: effects of production conditions and particle size. Chemosphere 145, 336–341.
Hug, S.J., Canonica, L., Wegelin, M., Gechter, D., Gunten, U.V., 2001. Solar oxidation and removal of arsenic at circum neutral pH in iron containing waters. Environ. Sci. Technol. 35, 2114–2121.
Karaca, S., Gurses, A., Ejder, M., Acikyildiz, M., 2004. Kinetic modeling of liquid-phase adsorption of phosphate on dolomite. J. Colloid Interface Sci. 277, 257–263.
Kim, J.W., Sohn, M.H., Kim, D.S., Sohn, S.M., Kwon, Y.S., 2001. Production of granular activated carbon from wastewalnut shell and its adsorptioncharacteristics for $Cu^{2+}$ ion. J. Hazard. Mater. B85, 301–315.
Krishna Veni, D., Kannan, P., Jebakumar Immanuel Edison, T.N., Senthilkumar, A., 2017. Biochar from green waste for phosphate removal with subsequent disposal. Waste Manage in press.
Krishnan, K.A., Haridas, A., 2008. Removal of phosphate from aqueous solutions and sewage using natural and surface modified coir pith. J. Hazard. Mater. 152, 527–535.
Kumar, P., Sudha, S., Chand, S., Srivastava, V.C., 2010. Phosphate removal from aqueous solution using coir-pith activated carbon. Sep. Sci. Technol. 45, 1–8.
Lim, S.F., Zheng, Y.M., Chen, J.P., 2009. Organic arsenic adsorption onto a magnetic sorbent. Langmuir 25, 4973–4978.
Loganathan, P., Vigneswaran, S., Kandasamy, J., Bolan, N.S., 2014. Removal and recovery of phosphate from water using sorption. Crit. Rev. Environ. Sci. Technol. 44, 847–907.
Michalekova-Richveisova, B., Fristak, V., Pipiska, M., Duriska, L., Moreno-Jimenez, E., Soja, G., 2017. Iron-impregnated biochars as effective phosphate sorption materials. Environ. Sci. Pollut. Res. Int. 24, 463–475.
Mohan, D., Sarswat, A., Singh, V.K., Alexandre-Franco, M., Pittman, C.U., 2011. Development of magnetic activated carbon from almond shells for trinitrophenol removal from water. Chem. Eng. J. 172, 1111–1125.
Neufeld, R.D., Thodos, G., 1969. Removal of orthophosphates from aqueous solutions with activated alumina. Environ. Sci. Technol. 3, 661–667.
Osouli-Bostanabad, K., Hosseinzade, E., Kianvash, A., Entezami, A., 2015. Modified nano-magnetite coated carbon fibers magnetic and microwave properties. Appl. Surf. Sci. 356, 1086–1095.
Pierce, M.L., Moore, C.B., 1982. Adsorption of arsenite and arsenate on amorphous iron hydroxide. Water Res. 16, 1247–1253.
Ren, J., Li, N., Li, L., An, J.K., Zhao, L., Ren, N.Q., 2015. Granulation and ferric oxides loading enable biochar derived from cotton stalk to remove phosphate from water. Bioresour. Technol. 178, 119–125.
Ruan, H.D., Frost, R.L., Kloprogge, J.T., Duong, L., 2002. Infrared spectroscopy of goethite dehydroxylation: III. FT-IR microscopy of in situ study of the thermal-transformation of goethite to hematite. Spectrochim. Acta Part A 58, 967–981.
Sarkar, S., Chatterjee, P.K., Cumbal, L.H., SenGupta, A.K., 2011. Hybrid ion exchanger supported nanocomposites: Sorption and sensing for environmental applications. Chem. Eng. J. 166, 923–931.
Shang, J.G., Pi, J.C., Zong, M.Z., Wang, Y.R., Li, W.H., Liao, Q.J.H., 2016. Chromium removal using magnetic biochar derived from herb-residue. J. Taiwan Inst. Chem. Eng. 68, 289–294.
Sun, J., Yang, Q., Wang, D.B., Wang, S.N., Chen, F., Zhong, Y., Y, K.X., Yao, F.B., Jiang, C., Li, S.B., Li, X.M., Zeng, G.M., 2017. Nickel toxicity to the performance and microbial community of enhanced biological phosphorus removal system. Chem. Eng. J. 313, 415–423.
USEPA. 1992. ESS Method 310.1: Ortho-phosphorus, dissolved automated, ascorbic acid. Environmental Sciences Section Inorganic chemistry unit, Wisconsin State Lab of Hygiene.
Wang, D.B., Yang, G.J., Li, X.M., Zheng, W., Wu, Y., Yang, Q., Zeng, G.M., 2012. Inducing mechanism of biological phosphorus removal driven by the aerobic/extended-idle regime. Biotechnol. Bioeng. 109, 2798–2807.
Wang, Z.F., Nie, E., Li, J.H., Yang, M., Zhao, Y.J., Luo, X.Z., Zheng, Z., 2011. Equilibrium and kinetics of adsorption of phosphate onto iron-doped activated carbon. Environ. Sci. Pollut. Res. Int. 19, 2908–2917.
Xie, T., Mo, C.R., Li, X.M., Zhang, J., An, H.X., Yang, Q., Wang, D.B., Zhao, J.W., Zhong, Y., Zeng, G.M., 2017. Effects of different ratios of glucose to acetate on phosphorus removal and microbial community of enhanced biological phosphorus removal (EBPR) system. Environ. Sci. Pollut. Res. 24, 4494–4505.
Xu, X., Gao, B.Y., Yue, Q.Y., Zhong, Q.Q., 2011. Sorption of phosphate onto giant reed based adsorbent: FTIR, Raman spectrum analysis and dynamic sorption/desorption properties in filter bed. Bioresour. Technol. 102, 5278–5282.
Yan, L.G., Yang, K., Shan, R.R., Yan, T., Wei, J., Yu, S.J., Yu, H.Q., Du, B., 2015. Kinetic, isotherm and thermodynamic investigations of phosphate adsorption onto core-shell $Fe_3O_4$@LDHs composites with easy magnetic separation assistance. J. Colloid Interface Sci. 448, 508–516.
Yao, Y., Gao, B., Inyang, M., Zimmerman, A.R., Cao, X.D., Pullammanappallil, P., Yang, L.Y., 2011. Removal of phosphate from aqueous solution by biochar derived from anaerobically digested sugar beet tailings. J. Hazard. Mater. 190, 501–507.

Yeoman, S., Stephenson, T., Lester, J.N., Perry, R., 1988. The removal of phosphorus during wastewater treatment: a review. Environ. Pollut. 49, 183–233.
Zeng, L., Li, X.M., Liu, J.D., 2004. Adsorptive removal of phosphate from aqueous solutions using iron oxide tailings. Water Res. 38, 1318–1326.
Zhang, G.S., Liu, H.J., Liu, R.P., Qu, J.H., 2009. Removal of phosphate from water by a Fe-Mn binary oxide adsorbent. J. Colloid Interface Sci. 335, 168–174.
Zhang, M., Gao, B., Yao, Y., Xue, Y.W., Inyang, M., 2012. Synthesis of porous MgO-biochar nanocomposites for removal of phosphate and nitrate from aqueous solutions. Chem. Eng. J. 210, 26–32.
Zhao, C., Shao, Q.J., Ma, Z.Q., Li, B., Zhao, X.J., 2016. Physical and chemical characterizations of corn stalk resulting from hydrogen peroxide presoaking prior to ammonia fiber expansion pretreatment. Ind. Crops Prod. 83, 86–93.
Zhao, J.W., Yang, Q., Li, X.M., Wang, D.B., Luo, K., Zhong, Y., Xu, Q.X., Zeng, G.M., 2015. Enhanced production of short-chain fatty acid from food waste stimulated by alkyl polyglycosides and its mechanism. Waste Manage. Res. 46, 133–139.
Zhong, Z.Y., Yang, Q., Li, X.M., Luo, K., Liu, Y., Zeng, G.M., 2012. Preparation of peanut hull-based activated carbon by microwave-induced phosphoric acid activation and its application in Remazol Brilliant Blue R adsorption. Ind. Crops Prod. 37, 178–185.